ACS Catalysis

Research Article

pubs.acs.org/acscatalysis

Mechanism of Cobalt-Catalyzed CO Hydrogenation: 2. Fischer–Tropsch Synthesis

Wei Chen, Ivo A. W. Filot, Robert Pestman, and Emiel J. M. Hensen*

Laboratory of Inorganic Materials Chemistry, Schuit Institute of Catalysis, Department of Chemical Engineering and Chemistry, Eindhoven University of Technology, P.O. Box 513, 5600 MB Eindhoven, The Netherlands

Supporting Information

ABSTRACT: Fischer–Tropsch (FT) synthesis is one of the most complex catalyzed chemical reactions in which the chain-growth mechanism that leads to formation of long-chain hydrocarbons is not well understood yet. The present work provides deeper insight into the relation between the kinetics of the FT reaction on a silica-supported cobalt catalyst and the composition of the surface adsorbed layer. Cofeeding experiments of $^{12}C_3H_6$ with $^{13}CO/H_2$ evidence that CH_x surface intermediates are involved in chain growth and that chain growth is highly reversible. We present a model-based approach of steady-state isotopic transient kinetic analysis measurements at FT conditions involving hydrocarbon products containing up to five carbon atoms. Our data show that the rates of chain growth and chain decoupling are much higher than the rates of monomer formation and chain termination. An important corollary of the microkinetic model is that the fraction of free sites, which is mainly determined by CO pressure, has opposing effects on CO consumption rate and chain-growth probability. Lower CO pressure and more free sites leads to increased CO consumption rate but decreased chain-growth probability because of an increasing ratio of chain decoupling over chain growth. The preferred FT condition involves high CO pressure in which chain-growth probability is increased at the expense of the CO consumption rate.

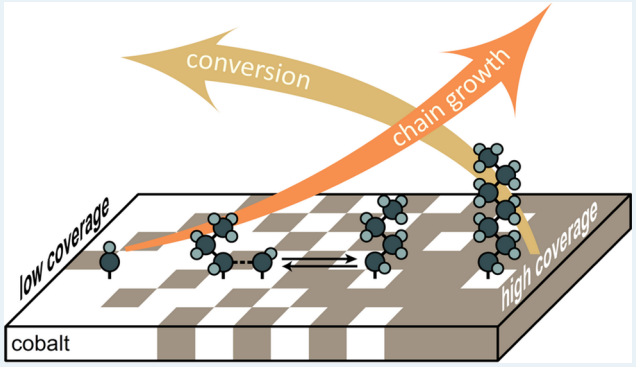

KEYWORDS: *Fischer–Tropsch, cobalt, mechanism, chain growth, SSITKA*

1. INTRODUCTION

The Fischer–Tropsch (FT) process encompasses a collection of chemical reactions that converts mixtures of CO and H_2 (synthesis gas) into liquid hydrocarbon fuels and chemicals.[1−4] It is currently primarily used to add value to large reserves of natural gas and coal by producing low-sulfur diesel or gasoline fuels. When natural gas is the feedstock for producing synthesis gas, cobalt is the preferred metal.[5] Alternatively, coal-derived synthesis gas is usually upgraded by iron-containing catalysts, mainly because of their higher water–gas shift activity.[6] In future energy scenarios, similar chemistry may also be used to upgrade resources such as biomass via synthesis gas[7,8] and to convert CO_2 with renewable H_2 into liquid fuels and chemicals.[9,10] Besides these practical aspects, catalytic FT synthesis of hydrocarbons continues to be of substantial scientific interest, because it involves a large number of elementary surface reaction steps, in which different sorts of surface intermediates participate, giving rise to CO dissociation, chain growth into long-chain olefins and paraffins and removal of oxygen in the form of water.[11−13]

The complexity of the FT reaction has led to an intense debate on the underlying mechanism, which is as old as this nearly one-century-old reaction itself.[14−16] The most-discussed one is arguably the way that the long-chain hydrocarbons are formed at the catalytic surface. It not only pertains to the chain-growth step itself but also to the mode of CO bond dissociation. The original idea proposed by Fischer and Tropsch was that metal carbide reacts with H_2 to produce methylene, acting as chain-growth monomer for long-chain hydrocarbon formation via polymerization.[2] This idea was later supported by experimental data[17−21] and has been retained up to now.[12,13] Alternatively, Pichler and Schulz proposed a chain growth pathway that proceeds via insertion of CO into the growing chains, followed by cleavage of the C–O bond.[22] Zhuo et al.[23] and Schweicher et al.[24] presented theoretical and experimental data, respectively, to support this mechanism. Also, other chain-growth monomers have been invoked, such as the formyl group.[25] So far, there is no consensus on the dominant mechanism, essentially because it is difficult to design experiments that allow distinguishing the two pathways.

Independent of the exact mechanism, a general feature of the FT reaction is that it proceeds as a surface polymerization process with in situ generation of chain-growth monomer, as reflected by the relative ratios of hydrocarbons of different

Received: August 14, 2017
Revised: September 24, 2017
Published: October 16, 2017

DOI: 10.1021/acscatal.7b02758
ACS Catal. 2017, 7, 8061−8071

length usually following a typical Anderson−Schulz−Flory (ASF) distribution.[26−28] Typically, this distribution is discussed in terms of a single parameter, the chain-growth probability α, defined as

$$\alpha = \frac{r_p}{r_p + r_t} \quad (1)$$

where r_p and r_t refer to the rates of propagation and termination of the hydrocarbon chain, respectively. As typically the aim of the FT process is to produce long-chain hydrocarbons, it is important to understand the kinetic aspects of this chain reaction in which monomer formation (initiation), chain growth (propagation), and chain termination are involved. These insights will help to improve activity and selectivity of FT catalysts.

Regarding FT reaction mechanism, most attention has been devoted to understanding CO bond dissociation on FT-active metals such as cobalt and ruthenium. Kinetically, CO bond dissociation should occur at a sufficient rate to provide enough monomers for chain growth.[12,13] As the activation barrier of CO dissociation on cobalt[29−32] and ruthenium[32,33] terraces is too high to be consistent with FT reactivity, H-assisted CO bond dissociation on terraces has been considered involving HCO[34] or HCOH[35−38] intermediates. This mechanism can explain the positive reaction order with respect to H_2 assuming that CO dissociation is the rate-determining step. The alternative view is that step-edges are the active sites involved in CO dissociation. Density functional theory (DFT) calculations have shown that stepped sites can dissociate CO with low barrier without the involvement of H atoms.[31−33] We have recently confirmed that reversible CO dissociation can occur on cobalt nanoparticles without the assistance of hydrogen and that this reaction involves a relatively small fraction of the cobalt metal surface.[39] An important kinetic implication of this earlier work is that the near-unity reaction order with respect to H_2 observed during CO methanation is not caused by rate-determining CO dissociation but, instead, by slow hydrogenation of C atoms relative to CO dissociation.[40]

In this work, we focus on the chain-growth mechanism over the same silica-supported cobalt catalyst. We provide support for the importance of CH_x species as chain-growth monomer and present experimental evidence for the earlier discussed hypothesis that chain growth is reversible.[41−44] The reversibility of chain-growth has profound implications on the relation between the composition of the surface adsorbed layer and the chain-growth probability. We employ steady-state isotopic transient kinetic analysis to investigate chain growth by carefully examining the coverage of carbon-containing reaction intermediates and transient responses of FT products. These unique data show that forward and backward chain-growth reactions are very fast in comparison to other elementary reaction steps including chain termination. The obtained steady-state and transient data are used to fit a simplified microkinetic model. Microkinetics simulations are used to understand in detail the influence of particular reaction steps on activity and selectivity. Specifically, we will demonstrate how CO consumption rate strongly decreases with the fraction of free sites, while the reverse holds true for the chain-growth probability.

2. EXPERIMENTAL SECTION

Preparation and Basic Characterization. The Co/SiO_2 catalyst prepared by incipient wetness impregnation method containing 17.1 wt % Co and 0.04 wt % Pt as determined by ICP−OES (SpectroBlue, Ametek Inc.), where Pt was used as reduction promoter. The catalysts were dried at 110 °C for 12 h and then calcined at 350 °C in static air for 2 h using a heating rate of 1 °C min^{-1}. Cobalt dispersion was measured by H_2-chemisorption on Micromeritics ASAP 2010 after reaction at 450 °C for 6 h. The average Co particle size is 15 nm as determined by TEM (FEI Tecnai 20, LaB6, 200 kV) and in situ XRD (D/max-2600, Rigaku). More details of experimental information on the basic characterization can be found in the Supporting Information.

In Situ FTIR Spectroscopy. FTIR spectra were recorded on Bruker Vertex V70v instrument. Typically, 15 mg of finely ground Co/SiO_2 catalyst was pressed into a self-supporting wafer and placed in an environmental transmission IR cell, which can be subjected to heating, cooling, gas dosing, and evacuation. Before IR measurements, the catalyst wafer was reduced in situ at 450 °C in a H_2 flow for 2 h. Subsequently, the cell was evacuated at 450 °C for 1 h to remove adsorbed hydrogen, followed by cooling to 35 °C in vacuum. Then, an IR spectrum was recorded as background for subsequent measurements. In a typical experiment, the cell was pressurized with 10 mbar CO using a needle valve. After 0.5 h, the cell was evacuated to a pressure lower than 10^{-5} mbar and heated to 300 °C at a rate of 5 °C min^{-1}. IR spectra were recorded every 5 °C at a resolution of 2 cm^{-1}. Each spectrum involved 16 accumulations that were averaged.

Steady-State Isotopic Transient Kinetic Analysis (SSITKA). Steady-state isotopic transient kinetic analysis (SSITKA) experiments were performed by a $^{12}CO/H_2 \rightarrow {}^{13}CO/H_2$ switch when steady-state CO conversion was obtained. The catalytic activity in steady state was determined online by analyzing the effluent gas on a Varian CP-3800 gas chromatograph equipped with TCD and FID detectors. The transient responses of Ne, $^{12}CH_4$, $^{13}CH_4$, ^{12}CO, and ^{13}CO were monitored by an online mass spectrometer (ESS, GeneSys Evolution) using m/z values of 22, 15, 17, 28, and 29, respectively. The transients of higher hydrocarbons were measured by a gas chromatograph equipped with a mass spectrometer (Shimazu, GCMS-QP 2010) and a 16-loop sample holder for storage of gas samples. In this way, the isotopic composition of higher hydrocarbons formed during a short reaction period can be analyzed. Detailed experimental and data analysis procedures can be found in the Supporting Information.

3. RESULTS AND DISCUSSION

SSITKA is uniquely suited to determine the coverage of reversibly adsorbed surface species during heterogeneous reactions.[45−47] In a companion paper, we already discussed CO hydrogenation to CH_4 at 260 °C on the same Co/SiO_2 catalyst. At this temperature, the formation of higher hydrocarbons is limited. The SSITKA data show that CO coverage under methanation conditions is relatively low (θ_{CO} < 0.30).[40] As a consequence, CO dissociation is intrinsically fast as compared to the hydrogenation of C and O species. It is important to establish how this picture changes when the temperature is decreased to 220 °C, which is a temperature close to the Fischer−Tropsch condition. We will first show

DOI: 10.1021/acscatal.7b02758
ACS Catal. 2017, 7, 8061−8071

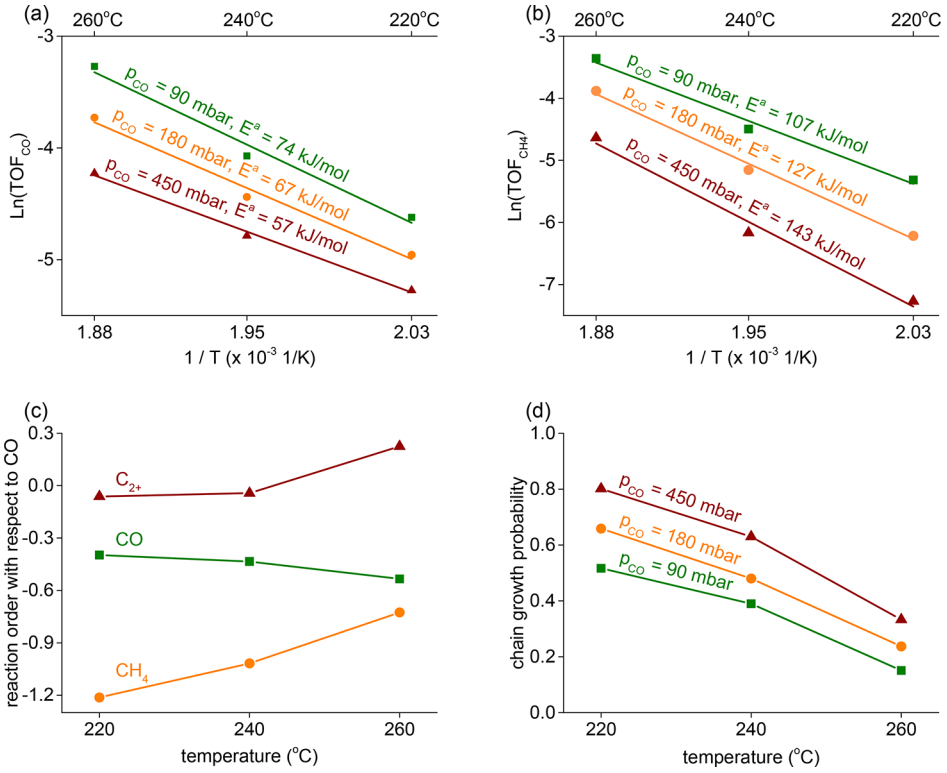

Figure 1. Kinetic parameters derived from steady-state measurement as a function of temperature (p_{CO} = 90–450 mbar, p_{H_2} = 900 mbar): (a) turnover frequency (TOF) of CO conversion, (b) TOF of CH_4 formation, (c) reaction order with respect to CO, and (d) chain-growth probability.

SSITKA data from which steady-state reaction rates, surface coverages, and other relevant kinetic parameters are derived. Then, we will provide evidence for the reversibility of chain growth, which is decoupling of chains into shorter chains and C_1 monomers, and the importance of high CO coverage to the FT condition. In the last part, we will discuss a microkinetic model fitted to experimental transient data and employ simulations based on this model to identify rate- and selectivity-controlling steps.

Steady-State Kinetics. Figure 1 shows the kinetic data derived from steady-state measurements (see Table S1 in the Supporting Information) at different temperatures. We include data obtained at 260 °C to highlight the influence of temperature. The overall apparent activation energy is about 74 kJ/mol at p_{CO} = 90 mbar, which is higher than the value of 57 kJ/mol obtained at p_{CO} = 450 mbar. It is also notable that the apparent activation energies based on the CH_4 formation rate are higher than those based on CO conversion. This is consistent with the higher CH_4 selectivity at lower CO partial pressure or when the temperature is increased. A necessary condition for FT synthesis is that CH_4 formation has a higher activation energy than C_{2+}-hydrocarbons formation. This difference also explains the observation that the reaction orders for CH_4 formation with respect to CO partial pressure are more negative than those for CO conversion. We observe that the chain-growth probability strongly decreases with temperature. Notably, the chain-growth probability is in the range of 0.52–0.85 under the conditions applied for model fitting (vide infra).

SSITKA experiments were carried out at 220 °C and 260 °C to determine steady-state CO and CH_x surface coverages as a function of CO and H_2 partial pressure. A typical SSITKA result following a $^{12}CO/H_2 \rightarrow {}^{13}CO/H_2$ switch at 220 °C is presented in Figure 2. Figure 3 reports the steady-state CO

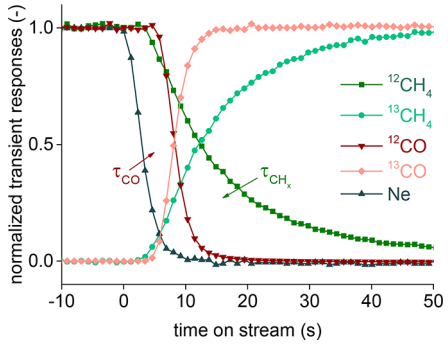

Figure 2. Typical transient responses following a $^{12}CO/H_2 \rightarrow {}^{13}CO/H_2$ switch. Condition at steady state: T = 220 °C, p_{H_2} = 900 mbar, p_{CO} = 180 mbar.

coverages obtained from SSITKA at 220 °C and 260 °C as a function of the CO and H_2 partial pressure. In agreement with literature,[38] the CO coverage increases with CO partial pressure following a Langmuir isotherm dependence. The CH_x coverage does not vary as strongly with CO partial pressure and a small decrease is noted. Figure 3b shows that the CO coverage only weakly depends on the H_2 partial pressure between 180 mbar and 1800 mbar, whereas the CH_x coverage is hardly affected. As outlined in our companion paper,[40] this result is consistent with the stronger adsorption of CO in comparison with H.

At 220 °C, the CO coverage reaches a maximum of 0.46 at a CO partial pressure of 450 mbar. A further increase does not further increase the CO coverage. The remainder of the surface is covered by CH_x species, growing chains (adsorbed C_{2+}), and, probably, irreversibly adsorbed species that cannot be determined by SSITKA and free sites. This result indicates that a CO coverage of about 0.5 ML is close to the saturated

DOI: 10.1021/acscatal.7b02758
ACS Catal. 2017, 7, 8061–8071

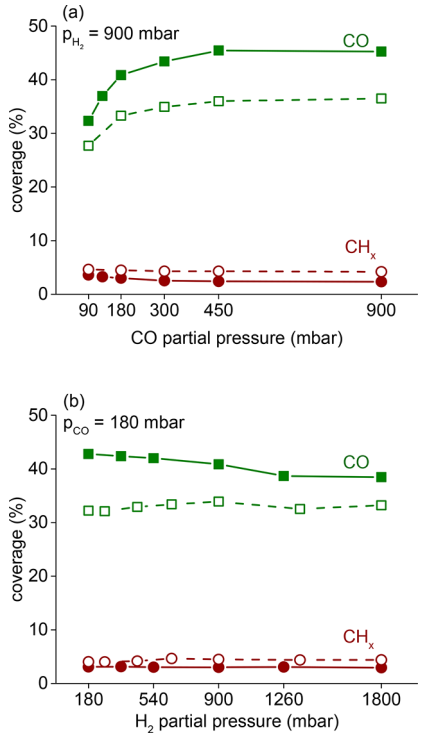

Figure 3. Coverage of CO (squares) and C_1 (circles) species as determined by SSITKA over the cobalt catalyst as a function of (a) CO partial pressure and (b) H_2 partial pressure at 220 °C (solid symbols) and 260 °C (open symbols).

CO coverage at this temperature. This is consistent with recent single crystal Co(0001) data using a Kelvin probe to determine CO coverage.[48] DFT calculations of the group of Saeys show that on the Co(0001) surface a maximum coverage of about 7/12 ML can be obtained.[49]

To gain insight into the fraction of free sites, which cannot be measured explicitly, we assume that the adsorption−desorption equilibrium of CO is established. Then, we can express the vacancy density, θ_v, as

$$\theta_v K_{CO} = \theta_{CO}/p_{CO} \quad (2)$$

where θ_{CO} is the CO coverage, K_{CO} the equilibrium constant of CO adsorption, which is assumed to be independent of surface coverage, and p_{CO} CO partial pressure. Using actual values for the applied CO partial pressure and the SSITKA-measured CO coverage leads to the result that the fraction of vacancies is reduced by a factor of 7 when the CO partial pressure increases from 90 mbar to 900 mbar, while this fraction only decreased by less than 20% when the H_2 partial pressure increases from 180 mbar to 1800 mbar. This is expected as CO binds much stronger to the Co surface than H. Importantly, within the range of conditions we study here, a decrease in the fraction of free sites is strongly correlated to the CO partial pressure, while it hardly depends on the H_2 partial pressure.

Based on this correlation, Figure 4 shows how chain-growth probability depends on $\theta_v K_{CO}$. It emphasizes the strong correlation between free sites and chain-growth probability. Kruse and co-workers linked higher chain-growth probability to higher CO coverage (and thus, CO partial pressure) in the framework of the CO insertion mechanism.[24] In the CO-insertion mechanism, CO dissociation provides the C_1 species that initiates chain growth. Thus, a decreased CO dissociation

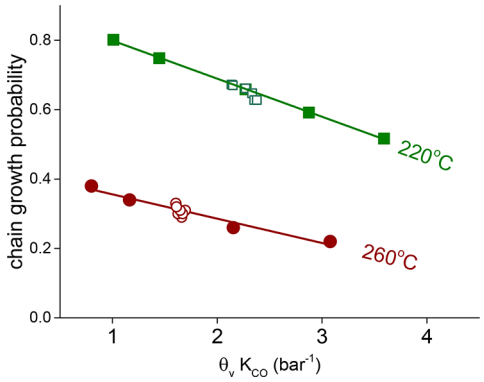

Figure 4. Chain-growth probability as a function of $\theta_v K_{CO}$ (= θ_{CO}/p_{CO}) at 220 °C (squares) and 260 °C (circles) as a function of CO partial pressure (denoted as solid symbols, p_{H_2} = 900 mbar, p_{CO} = 90−450 mbar) and varying H_2 partial pressure (denoted as open symbols, p_{H_2} = 180−1800 mbar, p_{CO} = 180 mbar), where θ_{CO} is the CO coverage determined by SSITKA and p_{CO} is CO partial pressure applied.

rate with increasing CO coverage is also consistent with the observation that CO consumption rate decreases. In the following section, we will discuss an alternative interpretation of these data following the carbide mechanism, involving reversibility of the chain-growth step.

Chain-Growth Monomer. The two essentially different reaction paths proposed for the chain-growth mechanism in the FT reaction differ by the chain-growth monomer, a CH_x species in the carbide mechanism[2] and CO in the CO-insertion mechanism.[22] First-principles-based microkinetics simulations on a stepped Ru surface operating under FT conditions have demonstrated that CH insertion is the dominant growth mechanism.[50] For both mechanisms, a necessary condition is that the chain-growth should be relatively fast compared to chain termination.[51]

We investigated the possibility of chain growth via CH_x species in the following manner. An in situ reduced catalyst was first exposed to CO flow at 260 °C for 0.5 h to deposit C atoms, and then evacuated (<10^{-5} mbar) at 300 °C for 1 h to remove adsorbed CO, eliminating a possible contribution of CO insertion into growing hydrocarbons. The absence of molecularly adsorbed CO was confirmed by IR spectra of adsorbed CO on the Co/SiO_2 catalyst recorded with increasing temperature (Figure 5a). After cooling to 200, 220, or 260 °C, the catalyst was exposed to a H_2 flow. As shown in Figure 5b, H_2-exposure at 260 °C led mainly to CH_4 and a small amount of C_2. When decreasing the hydrogenation temperature, the MS signals related to C_2 and C_3 hydrocarbons increased. Considering the absence of molecular CO, we conclude that the predeposited C species are involved in the formation of higher hydrocarbons. This further demonstrates that the carbide mechanism can contribute to chain growth in the FT reaction.

Cofeeding of ^{13}CO and $^{12}C_3H_6$. In most experimental kinetic studies of the FT reaction, it is assumed that the chain-growth step is irreversible. Quantum-chemical studies of chain growth on metallic cobalt and ruthenium surfaces according to the carbide mechanism show that the activation barriers for the insertion of the C_1 monomer into a growing chain and the reverse decoupling are of the same magnitude.[43] Microkinetics simulations based on the carbide mechanism predict that this

DOI: 10.1021/acscatal.7b02758
ACS Catal. 2017, 7, 8061−8071

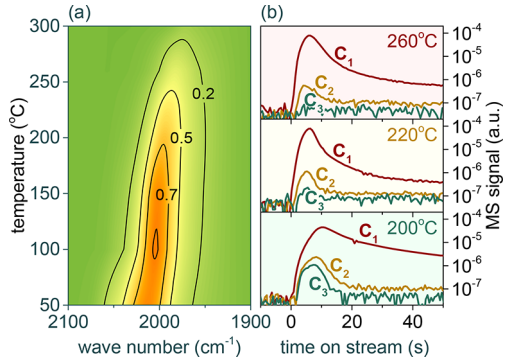

Figure 5. (a) Infrared spectra of CO adsorbed recorded in vacuum at increasing temperature showing that molecularly adsorbed CO is removed by evacuation at 300 °C. (b) Evolution of MS signals after H_2-exposure at 200 °C (bottom), 220 °C (middle), and 260 °C (top) over the cobalt catalyst, which was exposed to a CO flow at 260 °C for 30 min, followed by evacuation at 300 °C for 1 h.

reversibility should occur under FT conditions.[44] In order to experimentally verify the reversibility of chain growth, we carried out experiments in which $^{12}C_3H_6$ was cofed with $^{13}CO/H_2$.

Figure 6 shows that $^{12}CH_4$ appears in the hydrocarbon products mixture during ^{13}CO hydrogenation in the presence

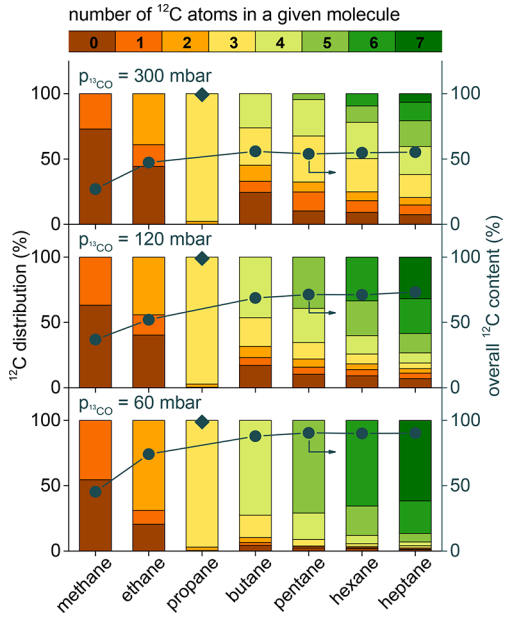

Figure 6. Isotopic content of alkane products when cofeeding $^{12}C_3H_6$ with $^{13}CO/H_2$ as a function of the CO partial pressure. The colors indicates the number of ^{12}C atoms in a given hydrocarbon. The markers show the total ^{12}C fraction for each product. Conditions: T = 220 °C, p_{H_2} = 600 mbar, $p^{12}{}_{C_3H_6}$ = 60 mbar.

of $^{12}C_3H_6$. This evidence confirms that the cobalt nanoparticle surface can decompose C−C bonds under FT conditions. Additionally, the simultaneous presence of ^{12}C and ^{13}C in C_2-products shows that the ^{12}C atoms obtained from $^{12}C_3H_6$ can be coupled to form higher hydrocarbons. We also observe that hydrocarbons with more than three C atoms contain different amounts of ^{12}C, indicating that $^{12}CH_x$ species are involved in the reaction as chain-growth monomers. Thus, this intermediate is both involved in chain growth and chain decoupling.

To gain an understanding into the chain-growth behavior of C_1 monomers derived from cofed $^{12}C_3H_6$, ASF-plots are presented in Figure 7. A mixture of $^{12}C_3H_6/H_2$ without CO

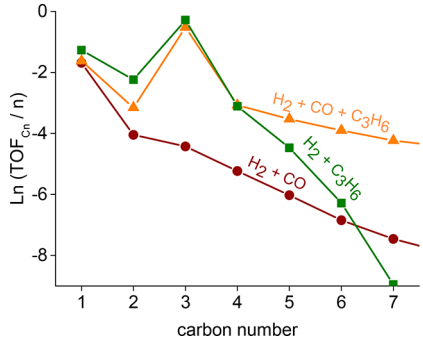

Figure 7. Logarithmic products distribution as a function of carbon number (ASF plot) obtained at 220 °C (squares: p_{H_2} = 600 mbar, $p^{12}{}_{C_3H_6}$ = 60 mbar; circles: p_{H_2} = 600 mbar, $p^{13}{}_{CO}$ = 60 mbar; triangles: p_{H_2} = 600 mbar, $p^{13}{}_{CO}$ = 60 mbar, $p^{12}{}_{C_3H_6}$ = 60 mbar).

gives rise to a hydrocarbons product distribution qualitatively similar to the distribution obtained with a CO/H_2 mixture. It should be noted that the C_3 products are an exception because of the cofeeding of propene. A substantial fraction of the $^{12}C_3H_6$ is hydrogenated to $^{12}C_3H_8$. This observation proves that similar chain growth as in the FT reaction occurs with $^{12}C_1$ species derived from $^{12}C_3H_6$. Figure 7 also shows that the addition of $^{12}C_3H_6$ to a $^{13}CO/H_2$ mixture facilitates the formation of higher hydrocarbons, both in terms of yield and chain-growth probability. Thus, the higher formation rate of higher hydrocarbons can be attributed to $^{12}C_1$ species obtained by $^{12}C_3H_6$ decoupling. As the $^{12}C_1$ species obtained by $^{12}C_3H_6$ decoupling are free of O, the CO-insertion mechanism cannot explain this specific case of chain growth. Considering furthermore that the product distribution in the presence of $^{12}C_3H_6$ (except for C_3) is almost similar to the product distribution obtained without cofed $^{12}C_3H_6$, we conclude that chain growth will proceed via an O-free C_1 species, that is to say via the carbide mechanism. The chain-growth probability values based on C_4−C_7 products obtained at different conditions are summarized in Table 1. Comparing the values with and without $^{12}C_3H_6$, one can see that the increase in chain-growth probability upon addition of $^{12}C_3H_6$ is limited by the increase in ^{13}CO partial pressure. Considering the fact that the CO partial pressure significantly influences the fraction of free sites,[52,53] both ^{13}CO dissociation and $^{12}C_3H_6$ decomposition

Table 1. Chain-Growth Probability (α, Based on C_4~C_7 Products) with and without 60 mbar Cofed $^{12}C_3H_6$ at Different ^{13}CO Partial Pressures[a]

$p^{13}{}_{CO}$ (mbar)	$p^{12}{}_{C_3H_6}$ (mbar)	α
60	0	0.44
120	0	0.62
300	0	0.81
0	60	0.23
60	60	0.66
120	60	0.76
300	60	0.84

[a]Condition: T = 220°C, p_{H_2} = 600 mbar.

DOI: 10.1021/acscatal.7b02758
ACS Catal. 2017, 7, 8061−8071

will be facilitated by a decrease in the CO partial pressure, and both reactions will supply chain-growth monomers, namely, $^{13}C_1$ and $^{12}C_1$ monomers, respectively. We observe in Figure 6 that the ^{12}C content rather than the ^{13}C content in the hydrocarbon products increases with decreasing ^{13}CO pressure. This suggests that the $^{12}C_3H_6$ decomposition profits more from free sites than $^{13}C-O$ bond scission. A kinetic implication is that, although C_1 supply via CO dissociation is promoted, an increasing fraction of free sites due to lowering of the CO partial pressure lowers the chain-growth probability due to faster chain decoupling.

Transient Response of FT Products. In the context of the FT reaction, SSITKA has been most frequently used at conditions resulting in high methane selectivity (i.e., $H_2/CO > 2$).[38,54−58] In this section, SSITKA will be used to investigate the transient behavior of the hydrocarbon products during the FT reaction, including CH_4 and higher hydrocarbons. Typical transients of the isotopologues of C_5H_{12} following a $^{12}CO/H_2 \rightarrow {}^{13}CO/H_2$ switch are presented in Figure 8. All responses of

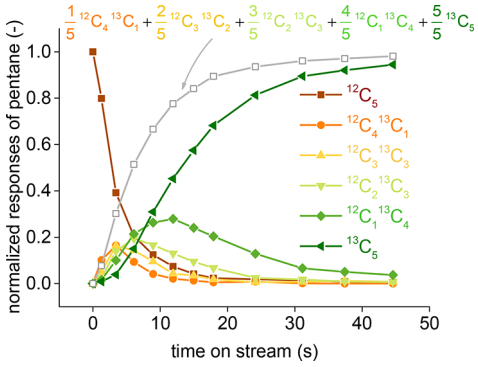

Figure 8. Normalized SSITKA responses of the isotopologues of pentane with different number of ^{13}C atoms. Transient was performed by switching from $^{12}CO/H_2$ to $^{13}CO/H_2$ at steady state. The open squares represent the evolution of ^{13}C fraction within pentane molecules (E_n), obtained by using the equation above. Conditions: T = 220 °C, p_{H_2} = 900 mbar, p_{CO} = 180 mbar.

partially labeled products display a maximum. The position of the maximum shifts in time with increasing isotope content of partially labeled C_5 hydrocarbon. The higher the ^{13}C content, the later the maximum occurs. Taking into account the ^{13}C content of all the isotopologues allows inspecting the evolution of ^{13}C fraction within a given product. An example is presented by the open symbols in Figure 8. This evolution is determined in the following manner

$$E_n(t) = \sum_{i=1}^{n} \frac{i}{n} N_{i,n}(t) \tag{3}$$

where n is the chain length of the given product, i the number of ^{13}C atoms in the product molecule, and $N_{i,n}$ refers to the normalized transient response of the C_n product with i ^{13}C atoms. The fractional ^{13}C evolution of C_1-C_5 alkanes are plotted in Figure 9. The result shows that the evolution of the ^{13}C content of C_1-C_5 alkanes with time on stream after the switch are almost identical and thus independent of chain length. The ^{13}C content of CH_4 can be directly correlated to the ^{13}C fraction of C_1 species on surface, as the formation of CH_4 does not involve C−C coupling steps but only CO dissociation and C hydrogenation. An implication of the

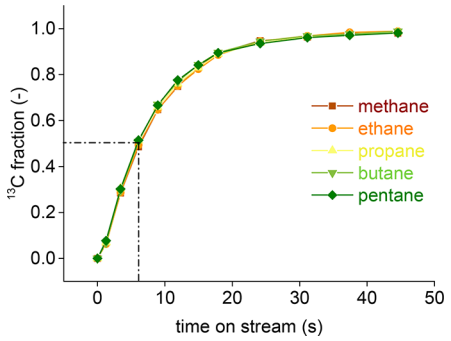

Figure 9. Evolution of ^{13}C content in FT products. Transient was performed by a switch from $^{12}CO/H_2$ to $^{13}CO/H_2$ at steady state. Conditions: T = 220 °C, p_{H_2} = 900 mbar, p_{CO} = 180 mbar.

overlapping of the ^{13}C evolution curves is that the ^{13}C content of all formed hydrocarbons is strongly correlated to the $^{13}C/^{12}C$ ratio of C_1 species on the surface. This further underpins that the C_1 species is the chain-growth monomer, rather than CO. Typically, the $^{13}CO/^{12}CO$ transient in SSITKA, which is directly correlated to the adsorbed $^{13}CO/^{12}CO$ ratio on the surface, is significantly shorter than the $^{13}CH_4/^{12}CH_4$ transient (Figure 2). If weakly adsorbed CO is the chain-growth monomer, as proposed by Schweicher et al. in the CO-insertion mechanism,[24] one expects more rapid introduction of ^{13}C fraction into C_{2+} products than in CH_4. The observation that the ^{13}C content evolution is independent of chain length of the hydrocarbon including CH_4 therefore demonstrates that CO insertion cannot be the dominant chain-growth mechanism. Regarding the process of chain-growth, the formation of a long-chain hydrocarbon will take more time than the formation of a shorter one. The chain-length-independent ^{13}C evolution suggests that the chain growth and decoupling steps are very fast in comparison to monomer formation. In this way, the ^{13}C content of the growing chains is dictated by that of the C_1 species. An important corollary of this finding is that the chain-growth rate is mainly limited by the supply of C_1 monomers under the FT condition on the cobalt catalyst. This is in agreement with microkinetics simulations showing that, within the carbide mechanism, chain growth may occur on sites with high CO coverage as long as the rate of chain growth is fast compared to the rate of chain monomer supply.[12,51] Together with the inverse correlation between the amount of free sites and the chain-growth probability (Figure 4) and the reversibility of chain growth evidenced in the previous section, we conclude that the chain-growth probability is largely controlled by the rate of chain growth vs chain decoupling. More free sites implies a higher rate of chain decoupling, while a higher rate of monomer formation leads to higher chain-growth probability. Recalling enhanced $^{12}C_3H_6$ decomposition by a decrease in the ^{13}CO partial pressure, the fraction of free sites influences chain decoupling more significantly than C−O scission. This issue will also follow from microkinetic modeling to be discussed below.

Figure 10 plots the transients of unlabeled and fully labeled C_1-C_5 alkanes following a $^{12}CO/H_2 \rightarrow {}^{13}CO/H_2$ switch. We observed that the transient of unlabeled short chain hydrocarbon is slower than that of longer ones and that $^{12}CH_4$ decays slowest among all unlabeled products. The fully labeled products appear in the other way around; that is, the transient responses of fully labeled products become slower with increasing carbon number. The noteworthy aspect is that the

DOI: 10.1021/acscatal.7b02758
ACS Catal. 2017, 7, 8061−8071

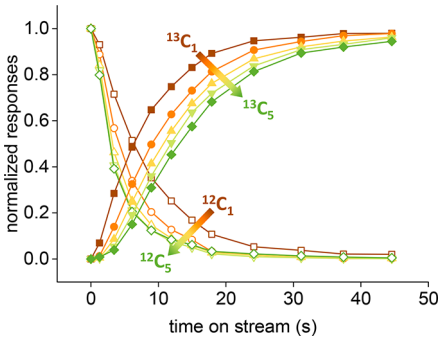

Figure 10. Normalized SSITKA responses of unlabeled (open symbols) and fully labeled (solid symbols) alkanes. The red lines are the response curves for methane. The arrows point into the direction with increasing length up to the response curves for pentane in green. Transient was performed by a switch from $^{12}CO/H_2$ to $^{13}CO/H_2$ at steady state. Conditions: T = 220 °C, p_{H_2} = 900 mbar, p_{CO} = 180 mbar.

responses of unlabeled and fully labeled isotopologues of all products cross each at the same time (~7 s). At this moment, as shown in Figure 9, the overall ^{13}C content is ~50% in all products. A similar observation was recently reported by Ledesma et al.[59] Its reason has been discussed above; that is, fast chain propagation/decomposition reactions result in a chain-length-independent ^{13}C evolution within a given product.

The residence time of unlabeled and fully labeled hydrocarbons measured at different CO partial pressure are presented as a function of chain length in Figure 11. The residence time of

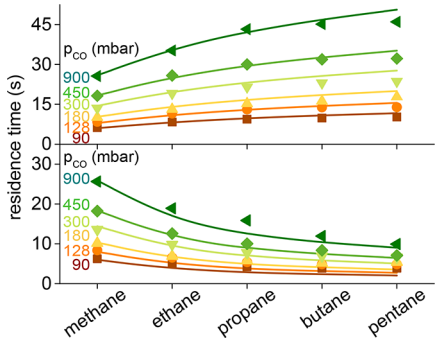

Figure 11. Residence time of fully labeled (upper) and unlabeled (bottom) alkanes measured at different CO partial pressure. The spots and lines represent the measurement and model fitting results, respectively. Transient was performed by a switch from $^{12}CO/H_2$ to $^{13}CO/H_2$ at steady state. Conditions: T = 220 °C, p_{H_2} = 900 mbar, p_{CO} = 90–900 mbar.

unlabeled products decreases with chain length, while the fully labeled products show an opposite trend in residence time. The physical meaning of the residence time of CH_4 is clear.[45,56−58] However, the meaning of the residence time of higher hydrocarbons is less evident, as the intermediates of long-chain hydrocarbon can be formed via multiple routes on the catalytic surface. For instance, C_2H_6 can be formed via either hydrogenation of adsorbed C_2 species, or C−C coupling followed by hydrogenation, implying that the measured residence time of C_2H_6 is a combination of several paths. In other words, it is not possible to directly derive intrinsic formation rate of C_{2+}-hydrocarbons as is customarily done for CH_4 on the basis of its residence time. Therefore, a model fitting approach is employed to extract kinetic parameters that intrinsically control the activity and selectivity of the FT reaction on the Co/SiO_2 catalyst.

Microkinetic Modeling. Based on the mechanistic insights described in the previous sections, a lumped kinetic model[44,60] was established and fitted with steady-state kinetic and SSITKA data obtained at the following conditions: p_{CO} = 90−900 mbar, p_{H_2} = 900 mbar, and T = 220 °C. The model, which is schematically shown in Figure 12, takes into account the

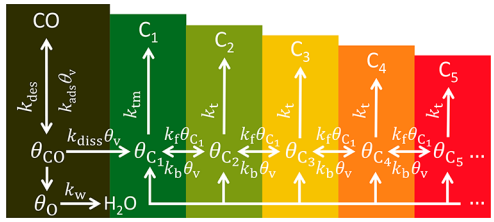

Figure 12. Schematic representation of the FT mechanism, where θ_{CO} presents adsorbed CO, θ_{Ci} adsorbed chains of i carbon atoms, C_i desorbed product of i carbon number, and θ_v vacant sites. k_{ads}/k_{des} presents the CO adsorption/desorption rate constants, k_{diss} the CO dissociation rate constant, k_{tm} the methane termination rate constant, k_t the chain termination rate constant, and k_f/k_b the forward/backward chain growth rate constants.

carbide mechanism and reversible chain growth. As compared to our earlier microkinetic model based on experimental transient kinetic data determined under methanation conditions,[40] hydrogenation steps are not explicitly involved but lumped into the rate constants. This is mainly done not only because involving hydrogenation steps into the reaction model would dramatically increase the number of unknown variables but also because the H coverage before and after the SSITKA switches remains unchanged.[60]

In the microkinetic model, CO adsorbs and desorbs with rate constants k_{ads} and k_{des}, respectively. Adsorbed CO dissociates with rate constant k_{diss} to yield C and O species. Notably, k_{diss} implicitly involves the H coverage for the C → CH_x reaction. The latter one is denoted by C_1 and is the chain-growth monomer. All chain-growth reaction steps, incorporating a C_1 species into a growing chain C_i, are considered to be reversible with rate constants k_f and k_b, respectively. These rate constants are assumed to be independent of the chain length. The intermediate that leads to CH_4 and the chain-growth monomer are assumed to be the same C_1 species. C_1 and C_i desorb as CH_4 and long-chain hydrocarbons in single lumped steps with rate constants k_{tm} and k_t, respectively. The value of k_{tm} is expected to be larger than that of k_t, as the selectivity of CH_4 is always higher than the expected CH_4 selectivity on the basis of the ASF distribution.[26−28] Adsorbed O is hydrogenated and removed as water with a lumped rate constant k_w. Readsorption of products is not considered in this model. The site balance is expressed by

$$\sum_{i=1}^{\infty} \theta_i + \theta_{CO} + \theta_O + \theta_v = 1 \tag{4}$$

The chain-growth probability is assumed to be chain-length independent and is determined by $\alpha = \theta_{C_{i+1}}/\theta_{C_i}$.[44,60] Accordingly, the site balance can be rewritten as

$$\frac{\theta_1}{1-\alpha} + \theta_{CO} + \theta_O + \theta_v = 1 \tag{5}$$

DOI: 10.1021/acscatal.7b02758
ACS Catal. 2017, 7, 8061−8071

Table 2. Rate Constants (s^{-1}) Determined by Model Fitting

p_{CO} (mbar)	k_{ads} [a]	k_{des}	k_{diss}	k_{tm}	k_t	k_f	k_b	k_w
90	3.7	0.033	1.30	0.60	0.22	4.1×10^3	2.1×10^3	0.163
137	3.6	0.034	1.31	0.52	0.18	4.5×10^3	2.1×10^3	0.135
180	3.4	0.036	1.32	0.43	0.16	4.7×10^3	2.2×10^3	0.143
300	2.9	0.038	1.39	0.28	0.13	4.7×10^3	2.4×10^3	0.144
450	2.8	0.039	1.38	0.19	0.10	4.8×10^3	2.5×10^3	0.148
900	2.6	0.042	1.40	0.079	0.076	5.1×10^3	2.6×10^3	0.149

[a] Unit: (s^{-1} bar^{-1})

Together with the site balance (eq 4), there are six differential equations that describe this model in terms of the evolution of surface coverage. In steady state, the differential equations are equal to zero.

$$\frac{d\theta_{CO}}{dt} = k_{ads}P_{CO}\theta_v - k_{des}\theta_{CO} - k_{diss}\theta_{CO}\theta_v = 0 \quad (6)$$

The C_1 and O coverages are given by

$$\frac{d\theta_{C_1}}{dt} = k_{diss}\theta_v\theta_{CO} - k_{tm}\theta_1 + (k_b\theta_v - k_f\theta_1)\frac{\theta_1}{1-\alpha} - k_f\theta_1^2 + k_b\theta_v\theta_1(\alpha - 1) = 0 \quad (7)$$

$$\frac{d\theta_O}{dt} = k_{diss}\theta_{CO}\theta_v - k_w\theta_O = 0 \quad (8)$$

As the coverage of growing chain is also constant, we can write

$$\frac{d\theta_{C_i}}{dt} = k_f\theta_1 + k_b\theta_v\alpha^2 - \alpha(k_f\theta_1 + k_b\theta_v + k_t) = 0 \quad (9)$$

The carbon balance yields

$$k_{ads}P_{CO}\theta_v - k_{des}\theta_{CO} - k_{tm}\theta_1 - \frac{k_f\theta_1}{(1-\alpha)^2} + k_f\theta_1 = 0 \quad (10)$$

Numerically solving this set of six equations will lead to the steady-state coverages θ_{CO}, θ_O, θ_{C_i}, and θ_v and the chain-growth probability. The experimental data to be fitted include transient data (data points in in Figures 11) and steady-state CO conversion rates and chain-growth probabilities measured at different CO partial pressure (90–900 mbar) at constant H_2 partial pressure (900 mbar) (Figure 1). The mathematical description of the SSITKA model and fitting procedure are described in Supporting Information.

The curves in Figure 11 show the good correspondence between experimental SSITKA data and model fitting. The rate constants determined by fitting the data obtained at different CO partial pressure are listed in Table 2. These data normalized based on the data obtained at the condition of p_{CO} = 90 mbar and p_{H_2} = 900 mbar are plotted in Figure 13 as a function of CO partial pressure. As expected, the rate constants of CH_4 formation (k_{tm}) and chain termination (k_t) decrease with rising CO pressure, because increasing CO pressure is accompanied by a decrease in the H coverage that is implicitly involved in k_{tm} and k_t. We observe that k_{tm} decreases more pronounced than k_t. This difference is in line with the experimentally observed more negative CO reaction order on the basis of CH_4 than on the basis of CO conversion. Note that the forward and backward chain-growth rates are orders of magnitude higher than the other rates. This is in accordance with a high exchange rate of C_1 monomer in the growing chain (vide infra). The rate constant for CO dissociation (k_{diss}) depends slightly on CO pressure, which can be explained by the implicit involvement of the C → CH_x reaction. The changes in CO adsorption and desorption can be explained by increasing lateral interactions at higher CO coverage, which also explains the minor changes of the other rate constants. It can be seen that the chain-growth and reversed chain-decoupling rates are much larger than the rate of monomer formation and termination. This is in line with the nearly identical evolution of isotopic inclusion in C_1–C_5 products as determined in the SSITKA experiment above (Figure 8).

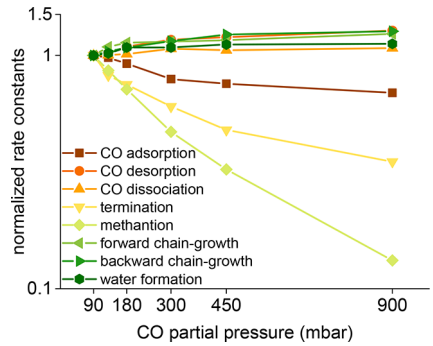

Figure 13. Rate constants determined by model fitting (T = 220 °C, p_{H_2} = 900 mbar, p_{CO} = 90–900 mbar). The data are normalized based on the values obtained at p_{CO} = 90 mbar.

Figure 14 shows model predictions of the steady-state kinetic parameters as a function of CO partial pressure. Figure 14a highlights the strong dependence of the CO consumption rate and chain-growth probability on CO coverage. Values for the degree of rate control (DRC)[61,62] are presented in Figure 14b. We also use a degree of chain-growth control (DCGC, detailed mathematical definition is provided in Supporting Information), which quantitatively describes the influence of individual elementary reaction steps on the chain-growth probability (Figure 14c). Finally, Figure 14d presents the predicted activity (expressed as turnover frequency, TOF), the chain-growth probability (α, defined as $\theta_{C_{i+1}}/\theta_{C_i}$) and the product distribution as a function of the free sites fraction. We note that a near-unity CO coverage in these models represents saturated CO adsorption in the practical situation rather than monolayer coverage of CO.

CO coverage markedly increases with CO pressure, resulting in a continuous loss of free sites. Concomitantly, the influence of CO adsorption on the overall rate becomes increasingly negative, which is consistent with the negative CO reaction order. CO adsorption inhibits the FT reaction by (i) hampering CO dissociation and (ii) slowing hydrogenation because of the

DOI: 10.1021/acscatal.7b02758
ACS Catal. 2017, 7, 8061–8071

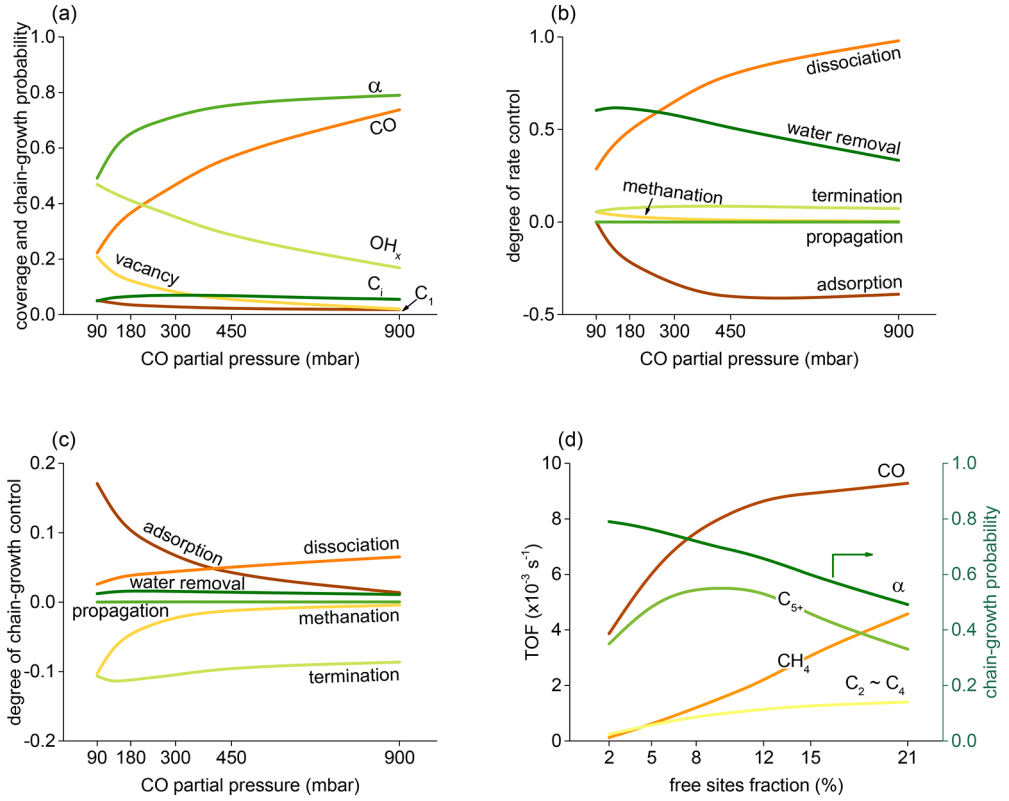

Figure 14. Microkinetics simulations at conditions of T = 220 °C, p_{H_2} = 900 mbar, p_{CO} = 90−900 mbar: (a) surface coverage and chain growth probability (α); (b) degree of rate control analysis; (c) degree of chain-growth control analysis; (d) turnover frequencies (TOFs) of CO consumption, CH_4 formation, C_2−C_4 formation, C_{5+} formation and chain-growth probability (α) as a function of the free sites fraction.

strong influence of CO adsorption on H coverage.[52,53] Compared with methanation conditions,[40] CO dissociation becomes the most rate-controlling step as there is a lack of free sites and competes with O removal.

The increase in chain-growth probability with CO partial pressure is caused by two factors, i.e., slow termination by hydrogenation and inhibited chain decoupling. The former one is confirmed by the relation between CO pressure and k_t and k_{tm} as shown in Figure 13. A nearly 1 order of magnitude decrease in the fraction of free sites (from 0.2 to 0.02) results in corresponding decrease of the chain-decoupling rate. In comparison, the increase in C_1 coverage (from 0.036 to 0.023 by SSITKA and from 0.051 to 0.019 predicted by microkinetics simulation) is relatively small, causing relatively small increase in chain-growth rate. Consequently, the net rate of chain-growth decreases as CO pressure increases. The positive correlation between chain-growth probability and CO adsorption becomes less pronounced when the fraction of free sites decreases. Then, CO dissociation becomes more important to the DCGC. The effect of O removal on the chain-growth probability is limited, as there are two opposing aspects. When more free sites become available by removing O, the CO dissociation rate and monomer supply increase, but it also enhances chain decoupling and hydrogenation. Accordingly, the DCGC values of O removal are only slightly positive. Expectedly, faster chain termination or methanation lowers chain-growth probability. It is noteworthy that changing the chain-growth rate constant (k_f), while fixing the equilibrium constant (k_f/k_b, according to the definition of the DCGC, see the Supporting Information for details) does not affect the chain-growth probability.

Taking into account the backward chain-growth rate, $r_{b,i}$, and the relation $\alpha_i = \theta_{C_{i+1}}/\theta_{C_i}$, we rewrite the expression of chain-growth probability at steady state in (see the Supporting Information for details)

$$\alpha_i = \frac{r_{f,i} - \alpha_i r_{b,i}}{r_{f,i} - \alpha_i r_{b,i} + r_{t,i}} \tag{11}$$

where the term $r_{f,i} - \alpha_i r_{b,i}$ represents the net rate of $C_i + C_1 \rightleftarrows C_{i+1}$. To analytically determine the influence of the rates of termination, forward and backward chain growth on the chain-growth probability, we calculate the derivative with respect to $r_{t,i}$ $r_{f,i}$, and $r_{b,i}$ as following.

$$\frac{\partial \alpha_i}{\partial r_{t,i}} = \frac{-r_{f,i} + \alpha_i r_{b,i}}{(r_{f,i} - \alpha_i r_{b,i} + r_{t,i})^2 + r_{b,i} r_{t,i}} \tag{12}$$

$$\frac{\partial \alpha_i}{\partial r_{f,i}} = \frac{r_{t,i}}{(r_{f,i} - \alpha_i r_{b,i} + r_{t,i})^2 + r_{b,i} r_{t,i}} \tag{13}$$

$$\frac{\partial \alpha_i}{\partial r_{b,i}} = \frac{-\alpha_i r_{t,i}}{(r_{f,i} - \alpha_i r_{b,i} + r_{t,i})^2 + r_{b,i} r_{t,i}} \tag{14}$$

Since k_f and k_b are 4 orders of magnitude larger than k_t, the rates of chain growth ($r_{f,i}$) and chain decoupling ($r_{b,i}$) are much higher than the rate of chain termination ($r_{t,i}$), while the net rate of chain growth ($r_{f,i} - \alpha r_{b,i}$), according to eq 10, is of the same order of magnitude as $r_{t,i}$. In this way, practical values of the chain-growth probability can be obtained. This approach shows the importance of chain decoupling on the chain-growth probability. Chain decoupling significantly decreases the values

DOI: 10.1021/acscatal.7b02758
ACS Catal. 2017, 7, 8061−8071

of $\frac{d\alpha_i}{dr_{t,i}}$, $\frac{d\alpha_i}{dr_{f,i}}$ and $\frac{d\alpha_i}{dr_{b,i}}$ through the term $r_{b,i}r_{t,i}$ in eqs 12-14. Notably, eqs 11-14 are consistent with the conventional definition of α_i (eq 1) when $r_{b,i}$ goes to zero.

As we discussed above, all the FT parameters can be directly or indirectly correlated to the amount of free sites. As a consequence, the reaction kinetics depends strongly on coverage as presented in Figure 11. As free sites play an important role in several crucial elementary steps in the FT reaction, their presence or absence is decisive in directing the selectivity toward desired FT products. As shown in Figure 14d, a certain fraction of free sites is needed to activate CO molecules, reflected by the negative reaction order with respect to CO. Concerning selectivity, reducing the fraction of free sites leads to high chain-growth probability by suppressing chain-decoupling. Thus, chain-growth probability and CO conversion rate are inversely correlated on the cobalt surface under FT reaction conditions. As commonly observed in catalysis,[50,63] the balance between activity and selectivity implies that there is an optimal surface composition leading to optimum performance in terms of higher hydrocarbons yield (see C_{5+} trace in Figure 14d). We find that CO pressure has the strongest influence on surface coverage. In industrial practice, CO pressures in the 10−15 bar are usually employed to achieve high chain-growth probability ($0.85 < \alpha < 0.95$) on a highly CO-covered surface.[64,65] As suggested by Figure 14d, high chain-growth probability comes at the expense of CO consumption rate.

CONCLUSIONS

The present work provides deeper insight into the relation between the kinetics of the FT reaction on a silica-supported cobalt catalyst and the composition of the surface adsorbed layer. We provide experimental data that unequivocally show that CH_x surface species are involved in chain growth and that chain growth is reversible. The latter chain-decoupling reaction benefits more from an increase in free sites than CO dissociation itself. SSITKA measurements at FT conditions involving hydrocarbons products up to C_5 show that the rates of chain growth and chain decoupling are much higher than the rates of monomer formation and chain termination. As reversible CO dissociation is slower than chain growth and the inclusion of isotopic C in growing chains is independent of chain length, CO cannot be the chain-growth monomer. A microkinetic model based on the carbide mechanism and involving reversible chain growth is fitted and used to understand several intricacies of the FT reaction. The fraction of free sites plays a crucial role in determining the CO consumption rate and the chain-growth probability. A high fraction of free sites leads to high CO consumption rate but decreases chain-growth probability because of a high ratio of chain decoupling over chain growth. Therefore, we understand the practical FT process, viz. high CO pressure, in terms of conditions that maximize the selectivity to heavy hydrocarbons (high chain-growth probability) at the expense of CO consumption rate.

ASSOCIATED CONTENT

Supporting Information

The Supporting Information is available free of charge on the ACS Publications website at DOI: 10.1021/acscatal.7b02758.

(1) Characterization; (2) catalytic tests and steady state isotopic transient experiments; (3) transient data analysis; (4) model fitting; (5) degree of rate control and degree of chain-growth control; (6) chain decoupling involved chain-growth probability (PDF)

AUTHOR INFORMATION

Corresponding Author

*E-mail: e.j.m.hensen@tue.nl.

ORCID

Emiel J. M. Hensen: 0000-0002-9754-2417

Notes

The authors declare no competing financial interest.

REFERENCES

(1) Fischer, F.; Tropsch, H. *Ber. Dtsch. Chem. Ges. B* **1923**, *56*, 2418−2428.
(2) Fischer, F.; Tropsch, H. *Ber. Dtsch. Chem. Ges. B* **1926**, *59*, 923−925.
(3) Dry, M. E. *Catal. Today* **2002**, *71*, 227−241.
(4) List, B. *Angew. Chem., Int. Ed.* **2014**, *53*, 8528−8530.
(5) Khodakov, A. Y.; Chu, W.; Fongarland, P. *Chem. Rev.* **2007**, *107*, 1692−1744.
(6) Dry, M. E. *Catal. Lett.* **1991**, *7*, 241−251.
(7) Jahangiri, H.; Bennett, J.; Mahjoubi, P.; Wilson, K.; Gu, S. *Catal. Sci. Technol.* **2014**, *4*, 2210−2229.
(8) Cortright, R. D.; Davda, R. R.; Dumesic, J. A. *Nature* **2002**, *418*, 964−967.
(9) Wang, W.-H.; Himeda, Y.; Muckerman, J. T.; Manbeck, G. F.; Fujita, E. *Chem. Rev.* **2015**, *115*, 12936−12973.
(10) Avanesian, T.; Gusmão, G. S.; Christopher, P. *J. Catal.* **2016**, *343*, 86−96.
(11) Bell, A. T. *Catal. Rev.: Sci. Eng.* **1981**, *23*, 203−232.
(12) Van Santen, R. A.; Ciobîcă, I. M.; van Steen, E.; Ghouri, M. M. *Adv. Catal.* **2011**, *54*, 127−187.
(13) Van Santen, R.; Markvoort, A. J.; Filot, I. A. W.; Ghouri, M. M.; Hensen, E. J. M. *Phys. Chem. Chem. Phys.* **2013**, *15*, 17038−17063.
(14) Rofer-DePoorter, C. K. *Chem. Rev.* **1981**, *81*, 447−474.
(15) Dry, M. E. *Appl. Catal., A* **1996**, *138*, 319−344.
(16) Claeys, M.; van Steen, E. *Stud. Surf. Sci. Catal.* **2004**, *152*, 601−680.
(17) Biloen, P.; Helle, J. N.; Sachtler, W. M. H. *J. Catal.* **1979**, *58*, 95−107.
(18) Ekerdt, J. G.; Bell, A. T. *J. Catal.* **1979**, *58*, 170−187.
(19) Brady, R. C., III; Pettit, R. *J. Am. Chem. Soc.* **1980**, *102*, 6181−6182.
(20) Brady, R. C., III; Pettit, R. *J. Am. Chem. Soc.* **1981**, *103*, 1287−1289.
(21) van Barneveld, W. A. A.; Ponec, V. *J. Catal.* **1984**, *88*, 382−387.
(22) Pichler, H.; Schulz, H. *Chem. Ing. Tech.* **1970**, *42*, 1162−1174.
(23) Zhuo, M.; Tan, K. F.; Borgna, A.; Saeys, M. *J. Phys. Chem. C* **2009**, *113*, 8357−8365.
(24) Schweicher, J.; Bundhoo, A.; Kruse, N. *J. Am. Chem. Soc.* **2012**, *134*, 16135−16138.
(25) Zhao, Y.-H.; Sun, K.; Ma, X.; Liu, J.; Sun, D.; Su, H.-Y.; Li, W.-X. *Angew. Chem., Int. Ed.* **2011**, *50*, 5335−5338.
(26) Schulz, H. *Catal. Today* **2013**, *214*, 140−151.
(27) Tavakoli, A.; Sohrabi, M.; Kargari, A. *Chem. Eng. J.* **2008**, *136*, 358−363.
(28) Henrici-Olivé, G.; Olivé, S. *Angew. Chem., Int. Ed. Engl.* **1976**, *15*, 136−141.
(29) Ge, Q.; Neurock, M. *J. Phys. Chem. B* **2006**, *110*, 15368−15380.
(30) Liu, J.-X.; Su, H.-Y.; Li, W.-X. *Catal. Today* **2013**, *215*, 36−42.
(31) Cheng, J.; Gong, X.; Hu, P.; Lok, C.; Ellis, P.; French, S. *J. Catal.* **2008**, *254*, 285−295.
(32) Shetty, S.; van Santen, R. A. *Catal. Today* **2011**, *171*, 168−173.
(33) Shetty, S.; Jansen, A. P. J.; van Santen, R. A. *J. Am. Chem. Soc.* **2009**, *131*, 12874−12875.

DOI: 10.1021/acscatal.7b02758
ACS Catal. 2017, 7, 8061−8071

(34) Mitchell, W. J.; Xie, J.; Jachimowski, T. A.; Weinberg, W. H. *J. Am. Chem. Soc.* **1995**, *117*, 2606−2617.
(35) Loveless, B. T.; Buda, C.; Neurock, M.; Iglesia, E. *J. Am. Chem. Soc.* **2013**, *135*, 6107−6121.
(36) Ojeda, M.; Nabar, R.; Nilekar, A. U.; Ishikawa, A.; Mavrikakis, M.; Iglesia, E. *J. Catal.* **2010**, *272*, 287−297.
(37) Qi, Y.; Yang, J.; Duan, X.; Zhu, Y.-A.; Chen, D.; Holmen, A. *Catal. Sci. Technol.* **2014**, *4*, 3534−3543.
(38) Yang, J.; Qi, Y.; Zhu, J.; Zhu, Y.-A.; Chen, D.; Holmen, A. *J. Catal.* **2013**, *308*, 37−49.
(39) Chen, W.; Zijlstra, B.; Pestman, R.; Hensen, E. *ChemCatChem* **2017**, DOI: 10.1002/cctc.201701203.
(40) Chen, W.; Pestman, R.; Zijlstra, B.; Filot, I. A. W.; Hensen, E. J. M. *ACS Catal.* 7 (11), DOI: 10.1021/acscatal.7b02757.
(41) Cheng, J.; Hu, P.; Ellis, P.; French, S.; Kelly, G.; Lok, C. *J. Catal.* **2008**, *257*, 221−228.
(42) Cheng, J.; Hu, P.; Ellis, P.; French, S.; Kelly, G.; Lok, C. M. *J. Phys. Chem. C* **2008**, *112*, 6082−6086.
(43) Filot, I. A. W.; Broos, R. J. P.; van Rijn, J. P. M.; van Heugten, G. J. H. A.; van Santen, R. A.; Hensen, E. J. M. *ACS Catal.* **2015**, *5*, 5453−5467.
(44) Markvoort, A. J.; van Santen, R. A.; Hilbers, P. A.; Hensen, E. J. *Angew. Chem., Int. Ed.* **2012**, *51*, 9015−9019.
(45) Shannon, S. L.; Goodwin, J. G. *Chem. Rev.* **1995**, *95*, 677−695.
(46) Ledesma, C.; Yang, J.; Chen, D.; Holmen, A. *ACS Catal.* **2014**, *4*, 4527−4547.
(47) Qi, Y.; Yang, J.; Chen, D.; Holmen, A. *Catal. Lett.* **2015**, *145*, 145−161.
(48) Weststrate, C. J.; van de Loosdrecht, J.; Niemantsverdriet, J. W. *J. Catal.* **2016**, *342*, 1−16.
(49) Zhuo, M.; Borgna, A.; Saeys, M. *J. Catal.* **2013**, *297*, 217−226.
(50) Filot, I. A. W.; van Santen, R. A.; Hensen, E. J. M. *Angew. Chem., Int. Ed.* **2014**, *53*, 12746−12750.
(51) Van Santen, R. A.; Markvoort, A. J.; Ghouri, M. M.; Hilbers, P. A. J.; Hensen, E. J. M. *J. Phys. Chem. C* **2013**, *117*, 4488−4504.
(52) Toyoshima, I.; Somorjai, G. A. *Catal. Rev.: Sci. Eng.* **1979**, *19*, 105−159.
(53) Winslow, P.; Bell, A. T. *J. Catal.* **1985**, *94*, 385−399.
(54) Lohitharn, N.; Goodwin, J. G., Jr. *J. Catal.* **2008**, *257*, 142−151.
(55) Lohitharn, N.; Goodwin, J. *J. Catal.* **2008**, *260*, 7−16.
(56) Yang, J.; Chen, D.; Holmen, A. *Catal. Today* **2012**, *186*, 99−108.
(57) Yang, J.; Tveten, E. Z.; Chen, D.; Holmen, A. *Langmuir* **2010**, *26*, 16558−67.
(58) Den Breejen, J. P.; Radstake, P. B.; Bezemer, G. L.; Bitter, J. H.; Frøseth, V.; Holmen, A.; Jong, K. P. d. *J. Am. Chem. Soc.* **2009**, *131*, 7197−7203.
(59) Ledesma, C.; Yang, J.; Blekkan, E. A.; Holmen, A.; Chen, D. *ACS Catal.* **2016**, *6*, 6674−6686.
(60) Van Santen, R. A.; Markvoort, A. J. *Faraday Discuss.* **2013**, *162*, 267−279.
(61) Stegelmann, C.; Andreasen, A.; Campbell, C. T. *J. Am. Chem. Soc.* **2009**, *131*, 8077−8082.
(62) Campbell, C. *J. Catal.* **2001**, *204*, 520−524.
(63) Cheng, J.; Hu, P. *J. Am. Chem. Soc.* **2008**, *130*, 10868−10869.
(64) Dry, M. E. In *Encyclopedia of Catalysis*; Horvath, I. T., Ed.; Elsevier: Amsterdam, 2003; Vol. 3, pp 347−401.
(65) Van de Loosdrecht, J. B.; Botes, F. G.; Ciobîcă, I. M.; Ferreira, A.; Gibson, P.; Moodley, D. J.; Saib, A. M.; Visagie, J. L.; Weststrate, C. J.; Niemantsverdriet, J. W. In *Reference Module in Chemistry, Molecular Sciences and Chemical Engineering: Comprehensive Inorganic Chemistry II*; Reedijk, J., Poeppelmeier, K., Eds.; Elsevier: Amsterdam, 2013; Vol. 7, pp 525−557.

DOI: 10.1021/acscatal.7b02758
ACS Catal. 2017, 7, 8061−8071